Missing Intensity Interpolation Using a Kernel PCA-Based POCS Algorithm and Its Applications

Takahiro Ogawa, *Member, IEEE* and Miki Haseyama, *Member, IEEE,*

***Abstract*—A missing intensity interpolation method using a kernel PCA-based projection onto convex sets (POCS) algorithm and its applications are presented in this paper. In order to interpolate missing intensities within a target image, the proposed method reconstructs local textures containing the missing pixels by using the POCS algorithm. In this reconstruction process, a nonlinear eigenspace is constructed from each kind of texture, and the optimal subspace for the target local texture is introduced into the constraint of the POCS algorithm. In the proposed method, the optimal subspace can be selected by monitoring errors converged in the reconstruction process. This approach provides a solution to the problem in conventional methods of not being able to effectively perform adaptive reconstruction of the target textures due to missing intensities, and successful interpolation of the missing intensities by the proposed method can be realized. Furthermore, since our method can restore any images including arbitrary-shaped missing areas, its potential in two image reconstruction tasks, image enlargement and missing area restoration, is also shown in this paper.**

***Index Terms*—Interpolation, kernel PCA, POCS, image enlargement, missing area restoration.**

I. Introduction

Interpolation of missing intensities affords numerous applications in image processing, such as image enlargement and restoration of missing areas. For a large class of image enlargement techniques, these are achieved by some kind of interpolation [1]–[4]; replication, bilinear and bicubic interpolations are the most popular choices and they are routinely implemented in commercial digital image processing software. Furthermore, interpolation techniques can be easily extended to restoration of missing areas in digital images [5]–[10]. Applications of interpolation such as removal of unnecessary objects, restoration of corrupted old films, and error concealment for video communication have been extensively studied.

In order to realize the above applications, many methods with goals of successful reconstruction of important visual features have been proposed. Generally, they are broadly classified into two categories, structural and texture reconstruction approaches. The former approaches focus on accurate edge reconstruction, and they are effective for pure structure images. However, since ordinary images also contain many textures, different approaches, texture reconstruction approaches, work better for those parts. In this paper, we focus on the texture reconstruction approach.

T. Ogawa and M. Haseyama are with the Graduate School of Information Science and Technology, Hokkaido University, Sapporo, 060-0814, JAPAN.

Manuscript received February 3, 2009; revised June 14, 2010.

In recent work, the study of kernel methods has developed rapidly and its achievements have become a center of attraction [11]. Kernel PCA (principal component analysis) is utilized for extraction of nonlinear visual features such as texture features in observed data. Furthermore, these features can be correctly expressed by a nonlinear subspace of which the dimension is much smaller than that of the input space. Kernel PCA has a useful characteristic compared to PCA. Generally, most images contain more low-frequency components than high-frequency components. From this characteristic, a low-dimensional eigenspace obtained by simple PCA can represent only such low-frequency components, and reconstruction results by PCA tend to be blurred. On the other hand, kernel PCA tends not to cause this problem, and its benefit can be confirmed in several papers [12]. Therefore, since the nonlinear eigenspace obtained by kernel PCA avoids the over-smoothness of reconstruction results compared to the eigenspace obtained by PCA, the use of the kernel PCA is effective for providing successful performance. Based on this advantage, several image reconstruction approaches including missing intensity interpolation and missing data estimation [12] have been proposed.

In most conventional methods, they require the assumption that arbitrary local areas within the target image have very similar texture features, that is, the target image contains only one type of texture. Thus, if the target image consists of various kinds of textures, the corrupted textures should be reconstructed from only the same kinds of textures. In this paper, since we focus on image enlargement and missing area restoration as applications of the missing intensity interpolation, we discuss the above point in these two study fields as follows.

Image Enlargement

In order to realize image enlargement, there have been proposed a number of attractive methods which depend on not only the intensity interpolation but also a learning-based (example-based) super-resolution [12]–[28]. The learning-based super-resolution recovers high-resolution images from their low-resolution observations by using other high-resolution images as training data, and representative methods were proposed by Freeman et al. [15], [16]. Their methods enable the estimation of unknown high-frequency components of high-resolution images from their mid-frequency components based on Markov networks.

Conventionally, several super-resolution methods based on PCA have been proposed for face hallucination [23], and they are improved by using kernel PCA [24]. Furthermore, Kim et al. proposed face hallucination and local patch-based super-

resolution of general images by using kernel PCA [12]. It is well known the PCA-based approach is suitable for images of a particular class such as face images and fingerprint images since this approach requires the assumption that all of the training images are in the same class. Then if the targets become arbitrary images, all of the training images are not necessarily in the same class, and their eigenspace cannot be obtained accurately. Thus, it is desirable that training images are first clustered, and the image enlargement is performed for each target image based on the eigenspace obtained by using the optimal cluster.

It should be noted that kernel PCA can be interpreted as a local PCA in a cluster structure. Kim et al. also explained at length that kernel PCA with a Gaussian kernel of suitable size could be interpreted as a local PCA in a cluster structure [12]. However, this characteristic of kernel PCA can be observed when the parameter of the Gaussian kernel is set to the optimal value. Therefore, if the parameter is not the optimal value, this characteristic may not be observed, and it becomes difficult to effectively utilize the cluster structure. From the above discussions, we can see the kernel PCA-based approach without using the clustering provides accurate performance if the optimal kernel (i.e. the Gaussian kernel with the optimal parameter) can be found, but it is too difficult to find the optimal one, which satisfies the cluster structure, for all images. Therefore, Hu et al. adopted the clustering-based scheme to realize the super-resolution based on nonlinear eigenspaces obtained from the clusters of training images by kernel PCA [29]. However, since this method performs the clustering of training images and the classification of target images based on the simple k-means scheme in the input space, its assignment is independent from the kernel PCA-based super-resolution. Then it does not always provide higher performance than those of the conventional methods.

Missing Area Restoration

There are several conventional methods, which focus on texture feature reconstruction, for achieving missing area restoration. Most algorithms reported in the literature reconstruct missing areas by utilizing statistical features of known textures within target images as training patterns. Generally, since the reconstruction of missing areas is an ill-posed problem, it is difficult to directly estimate the missing intensities. Thus, methods which approximate textures within target images in lower-dimensional subspaces and estimate the inverse projection for the corruption to reconstruct missing areas have been proposed. Specifically, Amano et al. proposed an effective PCA-based method for reconstructing missing textures by back projection for lost pixels [10]. Then missing areas within target images, which contain one type of texture, can be restored by using this method. However, when target images contain several kinds of textures, its low-dimensional eigenspace may not be able to represent those textures, accurately. Recently, many methods which utilize sparse representation approaches have intensively been studied [30]–[32]. By utilizing the sparse representation, the optimal signal-atoms for representing target signals can be adaptively selected from a dictionary. Thus, the problem in the above PCA-based approach of not being able to represent multiple kinds of textures tends to be solvable. Note that in this sparse representation approach, the optimal signal-atoms must be selected for target missing areas, and their representation coefficients must also be calculated accurately. Thus, the selection and calculation schemes become the most important issues. In the conventional methods, such optimal signal-atoms were selected from only the known neighboring intensities, and the representation coefficients were also calculated from those intensities, but these schemes were not necessarily optimal for target missing areas.

In this paper, a missing intensity interpolation method using a kernel PCA-based projection onto convex sets (POCS) algorithm and its applications are presented. The POCS algorithm has been applied to blocking artifact reduction in coded images as a nonlinear image restoration method [33]. In our method, missing intensities are interpolated by reconstructing local images including the missing pixels from the other known local images within the target image based on the POCS algorithm. The main contributions of this algorithm are twofold:

1) Introduction of nonlinear eigenspaces obtained from the known local images, which have the same kinds of textures, into the constraint of the POCS algorithm.

2) Adaptive selection of the optimal nonlinear eigenspace for the target local image based on the converged error of the POCS algorithm.

The main advantage of the first approach is that the nonlinear eigenspace enables correct approximation of the local images including the same kind of texture. Furthermore, the second approach provides a solution to the problem in the conventional methods of not being able to perform the adaptive and accurate selection of the optimal subspaces due to missing intensities. The errors monitored in the second approach correspond to the minimum distances between the target local image and the nonlinear eigenspaces utilized in the first approach even if intensities at the missing pixels within the target local image are unknown. Then these errors become better criteria for the selection of the optimal subspaces than those of the conventional methods.This is the biggest advantage of the proposed method. Therefore, the POCS algorithm, which introduces the optimal nonlinear eigenspace into its constraint, successfully reconstructs the textures within the target image, and its performance is better than the performances of conventional methods. Consequently, several applications such as image enlargement and restoration of missing areas can be realized by using our method, and the potential of our method is verified.

This paper is organized as follows. The POCS algorithm is explained in Section II. In Section III, the interpolation method based on the kernel PCA-based POCS algorithm is presented. In Section IV, applications of our interpolation method are shown. In Section V, the effectiveness of our method is verified by results of experiments. Concluding remarks are presented in Section VI.

II. POCS ALGORITHM

The POCS algorithm is explained in this section. The theory of POCS was first introduced to the field of image restoration

by Youla and Webb. In this algorithm, every known property of an original vector ν in the Hilbert space can be formulated as a corresponding convex set C_i $(i = 1, 2, \cdots, n)$. The original vector ν is then assumed to lie in the intersection of these convex sets, i.e.,

$$\nu \in C_0 = \bigcap_{i=1}^{n} C_i. \tag{1}$$

Since all of the known properties are captured in the intersection of all the convex sets, C_0, the problem of estimating the original vector ν from its n properties is equivalent to that of finding an element in C_0. If the projection operator P_i of the convex set C_i is given as

$$\|\nu - P_i\nu\| = \min_{\mu \in C_i} \|\nu - \mu\| \quad (i = 1, 2, \cdots, n), \tag{2}$$

the problem is recursively solvable. Therefore, the iterative equation given by

$$\nu_t = P_n P_{n-1} \cdots P_2 P_1 \nu_{t-1} \quad (t = 1, 2, \cdots) \tag{3}$$

will converge to a limiting point of the intersection $C_0 = \bigcap_{i=1}^{n} C_i$, as $t \to \infty$, for an arbitrary initial element.

The POCS framework ensures that the final solution is optimal mathematically. The optimality here is in the sense that the final solution satisfies all of the known constraints about the original vector.

III. KERNEL PCA-BASED POCS ALGORITHM FOR MISSING INTENSITY INTERPOLATION

A POCS-based interpolation method is presented in this section. Figure 1 shows an outline of the proposed method. First, the proposed method clips a local image f ($w \times h$ pixels) including missing pixels from the target image and interpolates their intensities by reconstructing f from the other known local images. For the following explanation, we denote the two areas, the intensities of which are unknown and known, as Ω and $\bar{\Omega}$, respectively within the target local image f. Note that there are many local images, the textures of which are quite different from that of the target local image f, within the target image. Such local images should not affect the reconstruction of the target local image f. Thus, in order to effectively reconstruct f from only the same kinds of known textures, the following two novel approaches are introduced into the POCS algorithm:

1) Introduction of nonlinear eigenspaces calculated from known local images, which contain the same textures, into the constraint of the POCS algorithm.

2) Adaptive selection of the optimal nonlinear eigenspace for the target local image f based on errors converged by the POCS algorithm.

The first approach enables accurate reconstruction of local images including the same kinds of textures. The second approach is necessary to select the nonlinear eigenspace of the same texture as that of the target local image f from only its known intensities. Then, by introducing these two approaches into the POCS algorithm, adaptive reconstruction of the target local image f by the optimal nonlinear eigenspace becomes feasible, and successful interpolation of the missing intensities should be achieved.

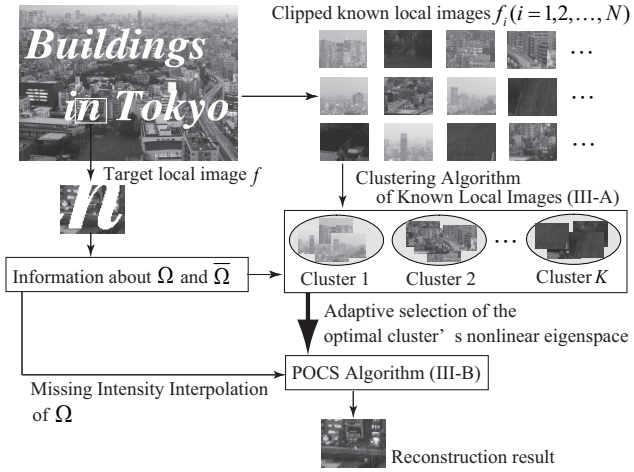

Fig. 1. Outline of the kernel PCA-based POCS algorithm for missing intensity interpolation.

In order to realize the above interpolation method, the known local images within the target image must first be assigned to some clusters before calculating their nonlinear eigenspaces. Thus, the clustering method is described in detail in III-A, and the method for interpolation of the missing intensities is presented in III-B.

A. Clustering Method of Known Local Images

In this subsection, clustering of known local images into K clusters is described. First, we clip N local images f_i ($w \times h$ pixels, $i = 1, 2, \cdots, N$) not including missing pixels at the same interval ($\tilde{w}_1 \times \tilde{h}_1$ pixels) in a raster scanning order from the target image. Next, for each local image f_i, two vectors $\mathbf{x}_i$ ($\in \mathbf{R}^{N_\Omega}$) and $\mathbf{y}_i$ ($\in \mathbf{R}^{wh-N_\Omega}$), whose elements are respectively raster scanned intensities in the corresponding areas of Ω and $\bar{\Omega}$, are defined, where N_Ω represents the number of pixels in Ω. Furthermore, the proposed method maps $\mathbf{x}_i$ and $\mathbf{y}_i$ into the feature spaces via nonlinear maps [11], and $\phi_{\mathbf{x}}(\mathbf{x}_i)$ and $\phi_{\mathbf{y}}(\mathbf{y}_i)$ are obtained. Note that the mapped results $\phi_{\mathbf{x}}(\mathbf{x}_i)$ and $\phi_{\mathbf{y}}(\mathbf{y}_i)$ are high-dimensional or infinite-dimensional, and it therefore may not be possible to calculate them directly. Fortunately, it is well known that the following computational procedures depend only on the inner products in the feature space, which can be efficiently obtained from a suitable kernel function [11]. In the proposed method, we utilize the Gaussian kernel since it is a default "general purpose kernel" in the kernel methods community [12].

From the vectors $\phi_{\mathbf{x}}(\mathbf{x}_i)$ and $\phi_{\mathbf{y}}(\mathbf{y}_i)$ obtained by the above procedures, we define a vector ϕ_i as follows:

$$\phi_i = \begin{bmatrix} \phi_{\mathbf{x}}(\mathbf{x}_i) \\ \phi_{\mathbf{y}}(\mathbf{y}_i) \end{bmatrix}. \tag{4}$$

Furthermore, the proposed method regards ϕ_i $(i = 1, 2, \cdots, N)$ as texture feature vectors and performs their clustering[1] that

[1]Initial clusters are obtained by the k-means method.

minimizes the following criterion:

$$E = \sum_{k=1}^{K} \sum_{j=1}^{M^k} \left\{ \|\mathbf{x}_j^k - \tilde{\mathbf{x}}_j^k\|^2 + \|\mathbf{y}_j^k - \tilde{\mathbf{y}}_j^k\|^2 \right\}, \tag{5}$$

where $\mathbf{x}_j^k$ and $\mathbf{y}_j^k$ ($j = 1, 2, \cdots, M^k$) are respectively $\mathbf{x}_i$ and $\mathbf{y}_i$ belonging to cluster k, and M^k is the number of elements in cluster k. Furthermore, given $\phi_j^k = \left[\phi_{\mathbf{x}}(\mathbf{x}_j^k)', \phi_{\mathbf{y}}(\mathbf{y}_j^k)'\right]'$ and $\tilde{\phi}_j^k = \left[\zeta_j^{k\prime}, \xi_j^{k\prime}\right]'$, they satisfy

$$\tilde{\phi}_j^k = \mathbf{U}^k \mathbf{U}^{k\prime} \left(\phi_j^k - \bar{\phi}^k\right) + \bar{\phi}^k, \tag{6}$$

where $\tilde{\mathbf{x}}_j^k$ and $\tilde{\mathbf{y}}_j^k$ in Eq. (5) respectively correspond to the pre-image [35] of ζ_j^k and ξ_j^k and satisfy $\phi_{\mathbf{x}}(\tilde{\mathbf{x}}_j^k) \cong \zeta_j^k$ and $\phi_{\mathbf{y}}(\tilde{\mathbf{y}}_j^k) \cong \xi_j^k$. In the above equation,

$$\mathbf{U}^k = \left[\mathbf{u}_1^k, \mathbf{u}_2^k, \cdots, \mathbf{u}_{D^k}^k\right] \quad \left(D^k < M^k\right) \tag{7}$$

is an eigenvector matrix of $\mathbf{\Xi}^k \mathbf{H}^k \mathbf{H}^k \mathbf{\Xi}^{k\prime}$, where $\mathbf{\Xi}^k = \left[\phi_1^k, \phi_2^k, \cdots, \phi_{M^k}^k\right]$ and $\mathbf{H}^k$ is the following centering matrix:

$$\mathbf{H}^k = \mathbf{I}^k - \frac{1}{M^k} \mathbf{1}^k \mathbf{1}^{k\prime}. \tag{8}$$

In Eq. (8), $\mathbf{I}^k$ is the $M^k \times M^k$ identity matrix and $\mathbf{1}^k = [1, 1, \cdots, 1]'$ is an $M^k \times 1$ vector. Note that in Eq. (7), D^k is the dimension of the eigenspace of cluster k, and it is set to the value whose cumulative proportion is larger than Th. In Eq. (6), $\bar{\phi}^k$ is a center vector of cluster k and is obtained as follows:

$$\bar{\phi}^k = \frac{1}{M^k} \mathbf{\Xi}^k \mathbf{1}^k. \tag{9}$$

In Eq. (7), the eigenvectors $\mathbf{u}_d^k$ ($d = 1, 2, \cdots, D^k$) are high-dimensional, and Eq. (6) cannot be calculated directly. Thus, we introduce a computation scheme using the kernel function into the calculation of Eq. (6). The eigenvector matrix $\mathbf{U}^k$ satisfies the following singular value decomposition:

$$\mathbf{\Xi}^k \mathbf{H}^k \cong \mathbf{U}^k \mathbf{\Lambda}^k \mathbf{V}^{k\prime}, \tag{10}$$

where $\mathbf{\Lambda}^k$ and $\mathbf{V}^k$ are respectively singular value and vector matrices. It should be noted that in the proposed method, the above equation is not directly calculated, and it is utilized for the following derivations. Therefore, $\mathbf{U}^k$ can be rewritten as follows:

$$\mathbf{U}^k \cong \mathbf{\Xi}^k \mathbf{H}^k \mathbf{V}^k \mathbf{\Lambda}^{-1}. \tag{11}$$

Then, from Eqs. (9) and (11), Eq. (6) can be rewritten as follows:

$$\tilde{\phi}_j^k \cong \mathbf{\Xi}^k \mathbf{T}^k \mathbf{\Xi}^{k\prime} \phi_j^k - \frac{1}{M^k} \mathbf{\Xi}^k \left(\mathbf{T}^k \mathbf{\Xi}^{k\prime} \mathbf{\Xi}^k - \mathbf{I}^k\right) \mathbf{1}^k, \tag{12}$$

where

$$\mathbf{T}^k = \mathbf{H}^k \mathbf{V}^k \mathbf{\Lambda}^{k^{-2}} \mathbf{V}^{k\prime} \mathbf{H}^k. \tag{13}$$

Furthermore, by noting $\mathbf{\Xi}^k = \left[\mathbf{\Xi}_{\mathbf{x}}^{k\prime}, \mathbf{\Xi}_{\mathbf{y}}^{k\prime}\right]'$ ($\mathbf{\Xi}_{\mathbf{x}}^k = [\phi_{\mathbf{x}}(\mathbf{x}_1^k), \phi_{\mathbf{x}}(\mathbf{x}_2^k), \cdots, \phi_{\mathbf{x}}(\mathbf{x}_{M^k}^k)]$ and $\mathbf{\Xi}_{\mathbf{y}}^k = [\phi_{\mathbf{y}}(\mathbf{y}_1^k), \phi_{\mathbf{y}}(\mathbf{y}_2^k), \cdots, \phi_{\mathbf{y}}(\mathbf{y}_{M^k}^k)]$), the following equation is obtained:

$$\begin{aligned} \begin{bmatrix} \zeta_j^k \\ \xi_j^k \end{bmatrix} &\cong \begin{bmatrix} \mathbf{\Xi}_{\mathbf{x}}^k \\ \mathbf{\Xi}_{\mathbf{y}}^k \end{bmatrix} \mathbf{T}^k \left[\mathbf{\Xi}_{\mathbf{x}}^{k\prime}, \mathbf{\Xi}_{\mathbf{y}}^{k\prime}\right] \begin{bmatrix} \phi_{\mathbf{x}}(\mathbf{x}_j^k) \\ \phi_{\mathbf{y}}(\mathbf{y}_j^k) \end{bmatrix} \\ &\quad - \frac{1}{M^k} \begin{bmatrix} \mathbf{\Xi}_{\mathbf{x}}^k \\ \mathbf{\Xi}_{\mathbf{y}}^k \end{bmatrix} \left(\mathbf{T}^k \left[\mathbf{\Xi}_{\mathbf{x}}^{k\prime}, \mathbf{\Xi}_{\mathbf{y}}^{k\prime}\right] \begin{bmatrix} \mathbf{\Xi}_{\mathbf{x}}^k \\ \mathbf{\Xi}_{\mathbf{y}}^k \end{bmatrix} - \mathbf{I}^k\right) \mathbf{1}^k \\ &= \begin{bmatrix} \mathbf{\Xi}_{\mathbf{x}}^k \\ \mathbf{\Xi}_{\mathbf{y}}^k \end{bmatrix} \psi_j^k, \end{aligned} \tag{14}$$

where

$$\begin{aligned} \psi_j^k &= \mathbf{T}^k \left(\mathbf{\Xi}_{\mathbf{x}}^{k\prime} \phi_{\mathbf{x}}(\mathbf{x}_j^k) + \mathbf{\Xi}_{\mathbf{y}}^{k\prime} \phi_{\mathbf{y}}(\mathbf{y}_j^k)\right) \\ &\quad - \frac{1}{M^k} \left\{\mathbf{T}^k \left(\mathbf{\Xi}_{\mathbf{x}}^{k\prime} \mathbf{\Xi}_{\mathbf{x}}^k + \mathbf{\Xi}_{\mathbf{y}}^{k\prime} \mathbf{\Xi}_{\mathbf{y}}^k\right) - \mathbf{I}^k\right\} \mathbf{1}^k. \end{aligned} \tag{15}$$

Thus, $\zeta_j^k \left(\cong \phi_{\mathbf{x}}(\tilde{\mathbf{x}}_j^k)\right)$ is obtained as follows:

$$\zeta_j^k \cong \mathbf{\Xi}_{\mathbf{x}}^k \psi_j^k. \tag{16}$$

From the above equation, we calculate $\|\mathbf{x}_j^k - \tilde{\mathbf{x}}_j^k\|^2$ in Eq. (5) as follows. Since we use the Gaussian kernel, the following equation is satisfied:

$$\begin{aligned} \|\phi_{\mathbf{x}}(\mathbf{x}_j^k) - \zeta_j^k\|^2 &= \phi_{\mathbf{x}}(\mathbf{x}_j^k)' \phi_{\mathbf{x}}(\mathbf{x}_j^k) + \zeta_j^{k\prime} \zeta_j^k - 2\phi_{\mathbf{x}}(\mathbf{x}_j^k)' \zeta_j^k \\ &\cong 1 + \psi_j^{k\prime} \mathbf{\Xi}_{\mathbf{x}}^{k\prime} \mathbf{\Xi}_{\mathbf{x}}^k \psi_j^k - 2\phi_{\mathbf{x}}(\mathbf{x}_j^k)' \mathbf{\Xi}_{\mathbf{x}}^k \psi_j^k. \end{aligned} \tag{17}$$

Finally,

$$\begin{aligned} \|\mathbf{x}_j^k - \tilde{\mathbf{x}}_j^k\|^2 &= -\sigma_{\mathbf{x}}^2 \log \left\{\phi_{\mathbf{x}}(\mathbf{x}_j^k)' \phi_{\mathbf{x}}(\tilde{\mathbf{x}}_j^k)\right\} \\ &= -\sigma_{\mathbf{x}}^2 \log \left\{\left(\phi_{\mathbf{x}}(\mathbf{x}_j^k)' \phi_{\mathbf{x}}(\mathbf{x}_j^k) + \phi_{\mathbf{x}}(\tilde{\mathbf{x}}_j^k)' \phi_{\mathbf{x}}(\tilde{\mathbf{x}}_j^k) \right.\right. \\ &\quad \left.\left. - \|\phi_{\mathbf{x}}(\mathbf{x}_j^k) - \phi_{\mathbf{x}}(\tilde{\mathbf{x}}_j^k)\|^2\right)/2\right\} \\ &\cong -\sigma_{\mathbf{x}}^2 \log \left\{\left(2 - \|\phi_{\mathbf{x}}(\mathbf{x}_j^k) - \zeta_j^k\|^2\right)/2\right\} \\ &= -\sigma_{\mathbf{x}}^2 \log \left\{\left(1 - \psi_j^{k\prime} \mathbf{\Xi}_{\mathbf{x}}^{k\prime} \mathbf{\Xi}_{\mathbf{x}}^k \psi_j^k + 2\phi_{\mathbf{x}}(\mathbf{x}_j^k)' \mathbf{\Xi}_{\mathbf{x}}^k \psi_j^k\right)/2\right\}, \end{aligned} \tag{18}$$

where $\sigma_{\mathbf{x}}^2$ is the parameter of the Gaussian kernel. In the same way as the calculation of $\|\mathbf{x}_j^k - \tilde{\mathbf{x}}_j^k\|^2$, $\|\mathbf{y}_j^k - \tilde{\mathbf{y}}_j^k\|^2$ can be also obtained as follows:

$$\|\mathbf{y}_j^k - \tilde{\mathbf{y}}_j^k\|^2 \cong -\sigma_{\mathbf{y}}^2 \log \left\{\left(1 - \psi_j^{k\prime} \mathbf{\Xi}_{\mathbf{y}}^{k\prime} \mathbf{\Xi}_{\mathbf{y}}^k \psi_j^k + 2\phi_{\mathbf{y}}(\mathbf{y}_j^k)' \mathbf{\Xi}_{\mathbf{y}}^k \psi_j^k\right)/2\right\}, \tag{19}$$

where $\sigma_{\mathbf{y}}^2$ is also a parameter of the Gaussian kernel.

In this way, we can assign the local images f_i ($i = 1, 2, \cdots, N$) to K clusters. The nonlinear eigenspace of each cluster k accurately approximates ϕ_j^k ($j = 1, 2, \cdots, M^k$) belonging to cluster k in the least-squares sense. Furthermore, we have regarded ϕ_j^k as the texture feature vectors of f_j^k, that is f_i belonging to cluster k. Then, noting the approximation error in the nonlinear eigenspace in Eq. (5), the proposed method can perform clustering of the local images based on their texture features.

B. Method for Interpolation of Missing Intensities

In this subsection, we present a method for interpolation of the missing intensities in the target local image f from the clustering results obtained by the previous subsection. First, we calculate the following vector ϕ_f in the same way as ϕ_i $(i = 1, 2, \cdots, N)$:

$$\phi_f = \begin{bmatrix} \phi_{\mathbf{x}}(\mathbf{x}) \\ \phi_{\mathbf{y}}(\mathbf{y}) \end{bmatrix}, \tag{20}$$

where $\mathbf{x}$ and $\mathbf{y}$ are respectively the unknown and known vectors whose elements correspond to the intensities in Ω and $\bar{\Omega}$ of f. Next, from this vector ϕ_f, the proposed method calculates a new vector $\hat{\phi}_f^k (= \left[\zeta^{k\prime}, \xi^{k\prime}\right]')$ satisfying the following two constraints to obtain the estimation result $\hat{\mathbf{x}}^k$ of the unknown vector $\mathbf{x}$.

[Constraint 1]
Since $\phi_{\mathbf{y}}(\mathbf{y})$ is the known vector calculated from the original intensities, it is fixed in the vector $\hat{\phi}_f^k$.

[Constraint 2]
In the feature space, the target vector $\hat{\phi}_f^k$ is in the nonlinear eigenspace spanned by the eigenvectors $\mathbf{u}_1^k, \mathbf{u}_2^k, \cdots, \mathbf{u}_{D^k}^k$ of cluster k. Therefore, $\hat{\phi}_f^k$ satisfies

$$\hat{\phi}_f^k = \mathbf{U}^k \mathbf{U}^{k\prime} \left(\hat{\phi}_f^k - \bar{\phi}^k\right) + \bar{\phi}^k. \tag{21}$$

From Eqs. (9) and (11), the above equation is rewritten as follows:

$$\hat{\phi}_f^k \cong \mathbf{\Xi}^k \mathbf{T}^k \mathbf{\Xi}^{k\prime} \hat{\phi}_f^k - \frac{1}{M^k} \mathbf{\Xi}^k \left(\mathbf{T}^k \mathbf{\Xi}^{k\prime} \mathbf{\Xi}^k - \mathbf{I}^k\right) \mathbf{1}^k. \tag{22}$$

The proposed method calculates the vector $\hat{\phi}_f^k$ that satisfies the above two constraints from the initial vector ϕ_f by utilizing the POCS algorithm. Specifically, these constraints are respectively utilized as the closed convex sets C_1 and C_2 in Eq. (1), and $\hat{\phi}_f^k$ is calculated by their projection operators P_1 and P_2 in Eq. (3). In this algorithm, if an intersection of the two closed convex sets does not exist, the result $\hat{\phi}_f^k$ satisfying both of the constraints cannot be obtained. In such a case, our method outputs the result satisfying Constraint 1.

If we define $\xi^k = \phi_{\mathbf{y}}(\mathbf{y})$ from Constraint 1, Eq. (22) is rewritten as

$$\begin{aligned} \begin{bmatrix} \zeta^k \\ \phi_{\mathbf{y}}(\mathbf{y}) \end{bmatrix} &\cong \begin{bmatrix} \mathbf{\Xi}_{\mathbf{x}}^k \\ \mathbf{\Xi}_{\mathbf{y}}^k \end{bmatrix} \mathbf{T}^k \left(\mathbf{\Xi}_{\mathbf{x}}^{k\prime} \zeta^k + \mathbf{\Xi}_{\mathbf{y}}^{k\prime} \phi_{\mathbf{y}}(\mathbf{y})\right) \\ &\quad - \frac{1}{M^k} \begin{bmatrix} \mathbf{\Xi}_{\mathbf{x}}^k \\ \mathbf{\Xi}_{\mathbf{y}}^k \end{bmatrix} \left\{\mathbf{T}^k \left(\mathbf{\Xi}_{\mathbf{x}}^{k\prime} \mathbf{\Xi}_{\mathbf{x}}^k + \mathbf{\Xi}_{\mathbf{y}}^{k\prime} \mathbf{\Xi}_{\mathbf{y}}^k\right) - \mathbf{I}^k\right\} \mathbf{1}^k. \end{aligned} \tag{23}$$

Therefore, ζ^k can be obtained by iterating the following calculation of ζ_t^k:

$$\begin{aligned} \zeta_t^k &\cong \mathbf{\Xi}_{\mathbf{x}}^k \mathbf{T}^k \left(\mathbf{\Xi}_{\mathbf{x}}^{k\prime} \zeta_{t-1}^k + \mathbf{\Xi}_{\mathbf{y}}^{k\prime} \phi_{\mathbf{y}}(\mathbf{y})\right) \\ &\quad - \frac{1}{M^k} \mathbf{\Xi}_{\mathbf{x}}^k \left\{\mathbf{T}^k \left(\mathbf{\Xi}_{\mathbf{x}}^{k\prime} \mathbf{\Xi}_{\mathbf{x}}^k + \mathbf{\Xi}_{\mathbf{y}}^{k\prime} \mathbf{\Xi}_{\mathbf{y}}^k\right) - \mathbf{I}^k\right\} \mathbf{1}^k, \end{aligned} \tag{24}$$

where ζ_0^k is an arbitrary vector.

The proposed method provides all of the constraints in the high-dimensional feature space and derives their projections as shown in Eq. (24), i.e. we newly introduce the derivation for the projections of the POCS algorithm in the feature space. In [34], the constraint of the known intensities was introduced in the input space. Thus, pre-image estimation [35] was performed by using the pseudo-inverse projection from the high-dimensional feature space to the input space for the projection of the POCS algorithm. Then since the projection to the constraint became the approximation, its error was caused in each iteration. This means the method in [34] could not strictly provide correct projections in the POCS algorithm. On the other hand, the proposed method does not utilize such approximation, theoretically, and more accurate projection can be obtained. Note that if the proposed method utilizes general PCA, the derivations of the proposed method and the method in [34] for the above two constraints become equivalent.

It is well known that an eigenspace calculated for sample data approximates them in the least-squares sense. Therefore, the nonlinear eigenspace utilized in Constraint 2 correctly approximates ϕ_j^k $(j = 1, 2, \cdots, M^k)$ belonging to cluster k. This means that this nonlinear eigenspace accurately reconstructs the textures in the same cluster since we regard ϕ_j^k as the texture feature vectors. Then, if the target ϕ_f belongs to cluster k, we can accurately estimate $\hat{\phi}_f^k$ and obtain accurate estimation results of the missing intensities. Unfortunately, we cannot know which cluster is the optimal for the target local image f by Eq. (5) since the vector $\mathbf{x}$ is unknown. Thus, in order to achieve the classification, the proposed method utilizes the following novel criterion as a substitute for Eq. (5):

$$\tilde{E}^k = \frac{\|\mathbf{y} - \hat{\mathbf{y}}^k\|^2}{wh - N_\Omega}, \tag{25}$$

where $\hat{\mathbf{y}}^k$ satisfies

$$\begin{aligned} \phi_{\mathbf{y}}(\hat{\mathbf{y}}^k) &\cong \mathbf{\Xi}_{\mathbf{y}}^k \mathbf{T}^k \left(\mathbf{\Xi}_{\mathbf{x}}^{k\prime} \zeta^k + \mathbf{\Xi}_{\mathbf{y}}^{k\prime} \phi_{\mathbf{y}}(\mathbf{y})\right) \\ &\quad - \frac{1}{M^k} \mathbf{\Xi}_{\mathbf{y}}^k \left\{\mathbf{T}^k \left(\mathbf{\Xi}_{\mathbf{x}}^{k\prime} \mathbf{\Xi}_{\mathbf{x}}^k + \mathbf{\Xi}_{\mathbf{y}}^{k\prime} \mathbf{\Xi}_{\mathbf{y}}^k\right) - \mathbf{I}^k\right\} \mathbf{1}^k. \end{aligned} \tag{26}$$

In the same way as Eq. (19), $\tilde{E}^k$ can be obtained as follows:

$$\tilde{E}^k \cong -\frac{\sigma_{\mathbf{y}}^2 \log\left\{\left(1 - \psi^{k\prime} \mathbf{\Xi}_{\mathbf{y}}^{k\prime} \mathbf{\Xi}_{\mathbf{y}}^k \psi^k + 2\phi_{\mathbf{y}}(\mathbf{y})' \mathbf{\Xi}_{\mathbf{y}}^k \psi^k\right)/2\right\}}{wh - N_\Omega}, \tag{27}$$

where

$$\begin{aligned} \psi^k &= \mathbf{T}^k \left(\mathbf{\Xi}_{\mathbf{x}}^{k\prime} \zeta^k + \mathbf{\Xi}_{\mathbf{y}}^{k\prime} \phi_{\mathbf{y}}(\mathbf{y})\right) \\ &\quad - \frac{1}{M^k} \left\{\mathbf{T}^k \left(\mathbf{\Xi}_{\mathbf{x}}^{k\prime} \mathbf{\Xi}_{\mathbf{x}}^k + \mathbf{\Xi}_{\mathbf{y}}^{k\prime} \mathbf{\Xi}_{\mathbf{y}}^k\right) - \mathbf{I}^k\right\} \mathbf{1}^k. \end{aligned} \tag{28}$$

Note that the vector $\hat{\mathbf{y}}^k$ becomes the same as $\mathbf{y}$ when an intersection of the two constraints exists. The criterion $\tilde{E}^k$ is the converged error of the POCS algorithm and also corresponds to the minimum distance between the target vector ϕ_f and the nonlinear eingepsace of cluster k in the input space. Therefore, this criterion $\tilde{E}^k$ as well as E in Eq. (5) is applicable for the classification of textures. Then, we can select the optimal cluster k^{opt} minimizing $\tilde{E}^k$ for ϕ_f even if the target local image f includes missing intensities.

As shown in the previous subsection and the above equations, the criteria for performing the clustering of the known local images f_i (Eq. (5)) and the classification of the target local image f (Eq. (27)) are calculated in the input space. This is because the intensities that we have to estimate are

in the input space. Thus, the proposed method introduces these criteria in the input space and enables their calculations without performing the pre-image approximation by the derivation schemes shown in Eqs. (5)–(19) and Eqs. (25)–(28). In [34], the criteria for the clustering and the classification are calculated in the high-dimensional feature space. In the point of view that our estimation results are in the input space, the criteria should be defined in the input space, and we therefore renew these criteria and their derivations in the proposed method. If the proposed method utilizes PCA without adopting any kernel methods, the derivations of the criteria in the proposed method and those in [34] become equivalent.

The proposed method outputs the result $\hat{\phi}_f^{k^{\rm opt}}$ obtained by cluster $k^{\rm opt}$ and regards its vector $\zeta^{k^{\rm opt}}$ as the estimation result of the missing intensities in the feature space. In the next step, we need to find a corresponding point of $\zeta^{k^{\rm opt}}$ in $\mathbf{R}^{N_\Omega}$ – this is the pre-image problem [35]. In order to solve it, our method calculates an approximation result $\mathbf{z}$ of $\hat{\mathbf{x}}^{k^{\rm opt}}$ by minimizing $\|\zeta^{k^{\rm opt}} - \phi_{\mathbf{x}}(\mathbf{z})\|^2$ over $\mathbf{z}\left(\in \mathbf{R}^{N_\Omega}\right)$. For the minimization, we use gradient decent with a starting point from the method of [35] in the same way as [12].

In this way, we can interpolate the missing intensities in the target local image f. The proposed method clips local images ($w \times h$ pixels) including missing intensities at the same interval ($\tilde{w}_2 \times \tilde{h}_2$ pixels) in a raster scanning order and reconstructs them by using our POCS algorithm. Note that each restored pixel has multiple estimation results if the clipping interval is smaller than the size of the local images. In this case, the proposed method regards the result minimizing Eq. (27) as the final one.

IV. APPLICATIONS OF OUR INTERPOLATION METHOD

This section shows several applications[2] of the missing intensity interpolation method presented in the previous section. The proposed method extends the range of several different applications since our POCS algorithm can interpolate arbitrary-shaped missing areas. We will demonstrate the potential of our algorithm in two image reconstruction tasks, image enlargement and missing area restoration.

A. Interpolation-based Image Enlargement

Interpolation-based image enlargement refers to the task of constructing a high-resolution (HR) image by interpolating intensities at non-integer coordinates of a low-resolution (LR) image. In order to realize this task by the proposed algorithm, we regard pixels at non-integer coordinates as missing pixels and interpolate their intensities. Note that the proposed method needs to clip local images ($w \times h$ pixels), the intensities of which are all known, from the target image for calculating their nonlinear eigenspaces. Unfortunately, we cannot clip such local images from the target image since all local images in the target image include missing pixels at non-integer coordinates. This means that the nonlinear eigenspaces of those local images cannot be directly calculated. Thus, we propose the following approach for estimating the nonlinear eigenspaces and thus achieving the image enlargement. Nonlinear eigenspaces calculated from local images ($w \times h$ pixels), which include only integer coordinate pixels in the LR image, are utilized for those of the HR image. It is well known that local images between two different resolution levels of a pyramid structure are similar to each other. Therefore, by utilizing the subspaces calculated from only the local images in the LR image, accurate estimation of the nonlinear eigenspaces of the HR image is expected. Then, interpolation-based image enlargement is realized by using the proposed method.

[2]In [34], it only focused on missing area restoration. On the other hand, the proposed missing intensity interpolation method in this paper is applied to image enlargement as well as missing area restoration for realizing various kinds of applications.

B. Missing Area Restoration

The restoration of missing areas is achieved by simply applying our POCS algorithm shown in the previous section to target images. Note that when missing areas exist all over the target image, we cannot obtain enough training patterns and accurate calculation of the nonlinear eigenspaces becomes difficult. In such a case, the proposed method again uses the results of reconstruction obtained by using our POCS algorithm for calculating the nonlinear eigenspace and iterates the clustering and interpolation procedures shown in III-A and III-B, respectively. Then, we renew the nonlinear eigenspaces utilized for the constraint and the reconstruction image and output the converged result. Consequently, the final reconstructed image can be obtained by using the proposed method.

V. EXPERIMENTAL RESULTS

In this section, we verify the performance of our interpolation method by applying it to the two applications. Experiments on interpolation-based image enlargement and missing area restoration are described in V-A and V-B, respectively.

A. Interpolation-based Image Enlargement

In this experiment, we utilized four color test images (24 bits/pixels) shown in Figs. 2(a)–(d). In order to obtain LR images, we downsampled these test images to the half or quarter size (Figs. 2(e)–(h)[3]) by using the sinc filter with the hamming window.

First, we focus the first test image shown in Figs. 2(a) and (e). We applied the conventional methods and the proposed method to the obtained LR image and estimated its enlargement results of size 320×240 pixels. For comparison, we adopted a local PCA-based method, the example-based super-resolution method [16], the kernel PCA-based super-resolution method [12], and the kernel PCA-based method including patch classification [29]. Note that the local PCA-based method is a simple PCA-based version of the proposed method without using the kernel method. The conventional method in [16] is a representative method of the learning-based super-resolution. Furthermore, the conventional method in [12] is also a representative method which utilizes the kernel PCA for performing the super-resolution, and its improvement

[3]In these figures, we simply enlarged the LR images to the size of the original images.

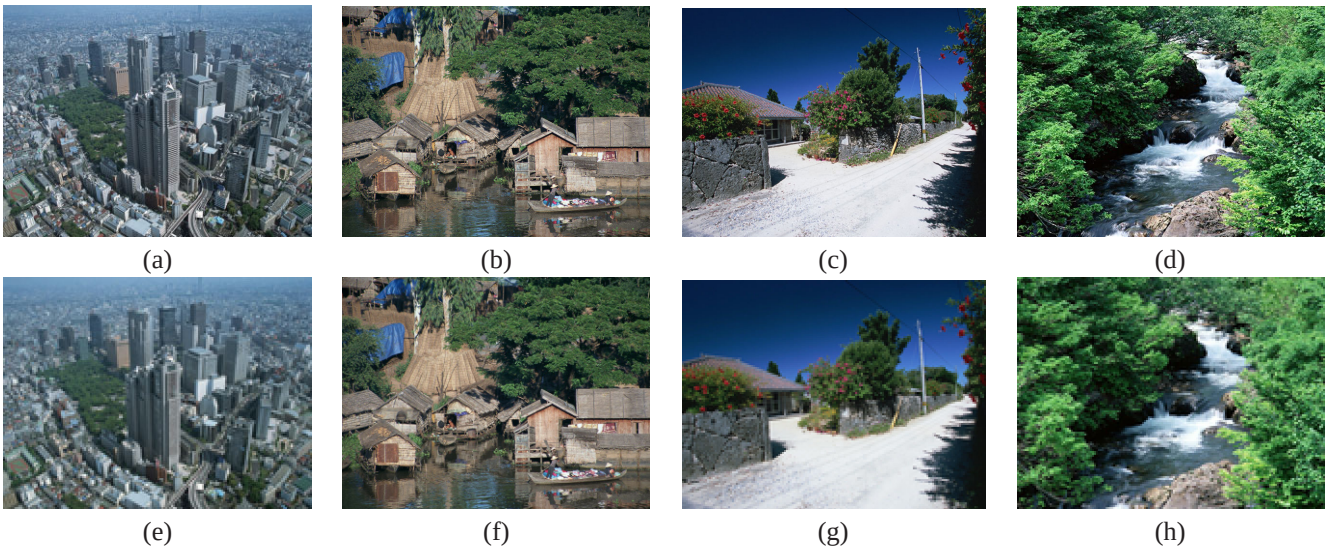

Fig. 2. Test images utilized in the verification of image enlargement performance: (a) Original HR test image 1 of size 320×240 pixels, (b) Original HR test image 2 of size 640×480 pixels, (c) Original HR test image 3 of size 640×480 pixels, (d) Original HR test image 4 of size 640×480 pixels, (e) LR image of (a) (160×120 pixels), (f) LR image of (b) (320×240 pixels), (g) LR image of (c) (160×120 pixels), (h) LR image of (d) (160×120 pixels).

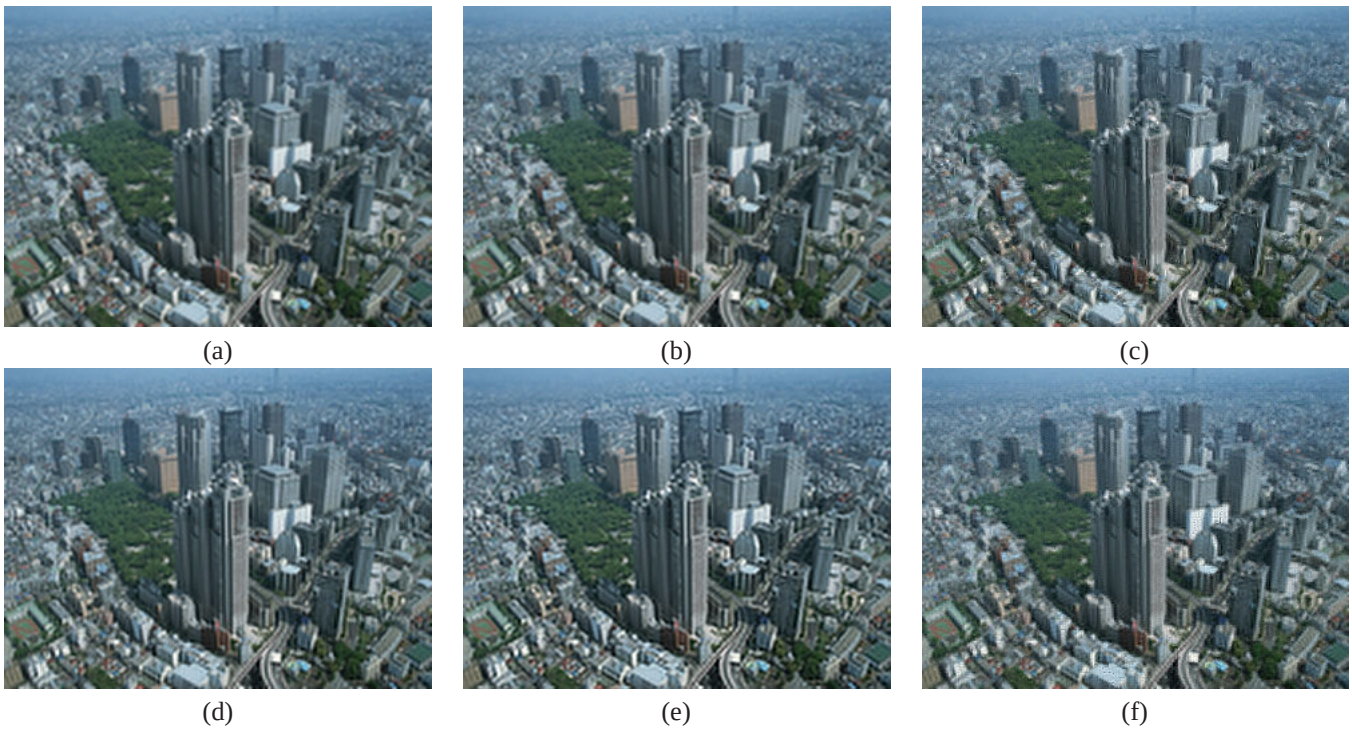

Fig. 3. Comparison of results (320×240 pixels) obtained by using different image enlargement methods (Test image 1): (a) Result of reconstruction by sinc interpolation, (b) Result of reconstruction by the local-PCA based method, (c) Result of reconstruction by the conventional method [16], (d) Result of reconstruction by the conventional method [12], (e) Result of reconstruction by the conventional method [29], (f) Result of reconstruction by the proposed method.

can be achieved in [29]. Therefore, these conventional methods are suitable for the comparison of the proposed method. Note that these example-based super-resolution methods [16], [12], [29] need training HR images for obtaining HR patches. Thus, in this experiment, we utilized patches clipped from the target LR image as training data, and it is the same approach as the proposed method for performing fair comparison.

In Fig. 3(a), we show the enlargement result obtained by the same filter used in the downsampling process, which is the most traditional approach. Next, Figs. 3(b)–(f) show the enlargement results respectively obtained by the local PCA-based method, the conventional methods [16], [12], [29], and our image enlargement approach shown in IV-A[4]. Note that we set the parameters of the proposed method as follows:

[4]In Figs. 3–8, the enlarged results obtained by the conventional and proposed approaches were high-boost filtered for better comparison.

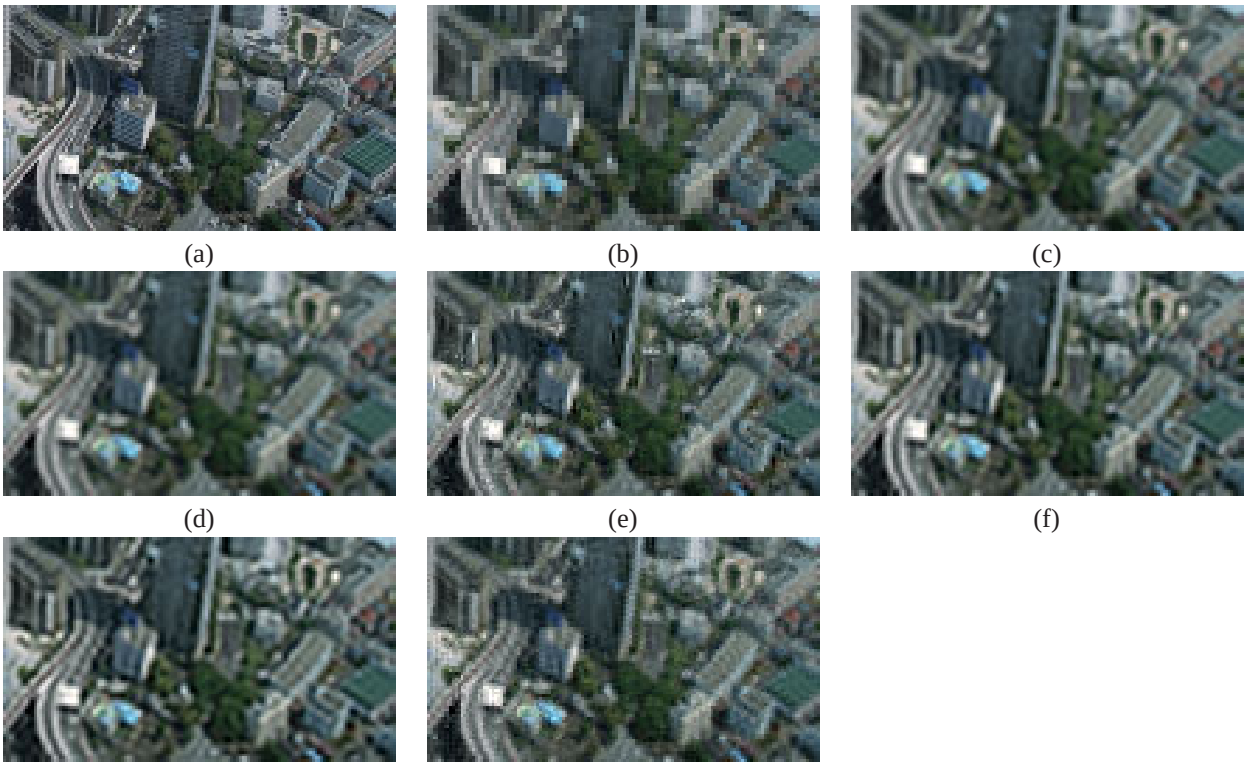

Fig. 4. (a) Zoomed portion of Fig. 2(a), (b) Zoomed portion of Fig. 2(e), (c) Zoomed portion of Fig. 3(a), (d) Zoomed portion of Fig. 3(b), (e) Zoomed portion of Fig. 3(c), (f) Zoomed portion of Fig. 3(d), (g) Zoomed portion of Fig. 3(e), (h) Zoomed portion of Fig. 3(f).

$w = 8$, $h = 8$, $\tilde{w}_1 = 2$, $\tilde{h}_1 = 2$, $\tilde{w}_2 = 4$, $\tilde{h}_2 = 4$, $K = 8$, and Th = 0.8. Furthermore, for color images, our method and the conventional methods were only applied to the luminance component, and two chroma components were enlarged by the same filter used in the downsampling process. From the zoomed portions shown in Fig. 4, we can see that the proposed method preserves the sharpness more successfully than do the conventional methods. The effectiveness of the proposed method can also be confirmed in Figs. 5–8. Note that in Figs. 6–8, the magnification factor of the enlargement is set to four. As the magnification factor becomes larger, the difference between the proposed method and the conventional methods also becomes significant.

From the obtained results, the proposed method keeps sharpness in the HR images more successfully than the conventional methods. The proposed method utilizes the kernel PCA to capture the nonlinear structure of texture features and enables the representation of local images keeping high-frequency components in the low-dimensional subspaces. From the results obtained by the local-PCA based method and the proposed method, we can also see our method preserves sharpness, successfully. Furthermore, in order to perform the adaptive texture reconstruction, the proposed method performs the classification of the target local images into the optimal cluster, i.e., the nonlinear eigenspace which is the optimal for each cluster can be utilized to estimate the missing intensities. In the conventional method [29], the classification scheme was also adopted. However, its scheme is based on the k-means method and independent from the kernel PCA-based super-resolution process. As shown in the previous section, the criteria utilized for the clustering of training images and the classification of the target local images in our method are suitable for the missing intensity interpolation. Then our method realizes more accurate performance.

Finally, as shown in Tables I and II, we show the PSNR and the SSIM index [36] obtained from the results of the proposed method and the conventional methods. Although the proposed method and the conventional methods [12], [29] keep the sharpness more successfully than the other methods, i.e., Sinc interpolation and the local PCA-based method, the PSNR cannot reflect the perceptual quality from Table I. Then Sinc interpolation which provides the most blurred results almost has the highest values. On the other hand, the SSIM index can provide the successful measure which is similar to the subjective evaluation in Figs. 3-8. Then the proposed method and the conventional methods [12], [29] almost have higher values than the other methods. Furthermore, among these three methods, the proposed method has the highest values for all the test images. Therefore, our method realizes successful resolution enhancement subjectively and quantitatively. It should be noted that since our method performs block-based procedures, its results suffer from some artifacts. However, it is expected that this problem will be solved by using some deblocking filters.

B. Missing Area Restoration

In this experiment, we utilized three color texture images (24-bit color levels) as shown in Figs. 9(a)–(c). Figure 10(a)

Fig. 5. Comparison of results by the conventional and proposed methods (Test image 2): (a) Zoomed portion of Fig. 2(b), (b) Zoomed portion of Fig. 2(f), (c) Zoomed portion of reconstruction result by sinc interpolation, (d) Zoomed portion of reconstruction result by the local-PCA based method, (e) Zoomed portion of reconstruction result by the conventional method [16], (f) Zoomed portion of reconstruction result by the conventional method [12], (g) Zoomed portion of reconstruction result by the conventional method [29], (h) Zoomed portion of reconstruction result by the proposed method.

TABLE I
IMAGE ENLARGEMENT PERFORMANCE COMPARISON (PSNR) OF THE PROPOSED METHOD AND THE CONVENTIONAL METHODS.

Test image	Sinc interpolation	Local PCA	Reference [16]	Reference[12]	Reference [29]	**Proposed method**
Fig. 2(a)	25.15	25.29	23.89	25.09	24.81	**24.98**
Fig. 2(b)	25.57	25.49	23.93	25.02	24.40	**25.07**
Fig. 2(c)	23.30	23.15	21.33	22.61	22.35	**23.83**
Fig. 2(d)	18.61	18.65	16.55	18.32	17.67	**18.50**

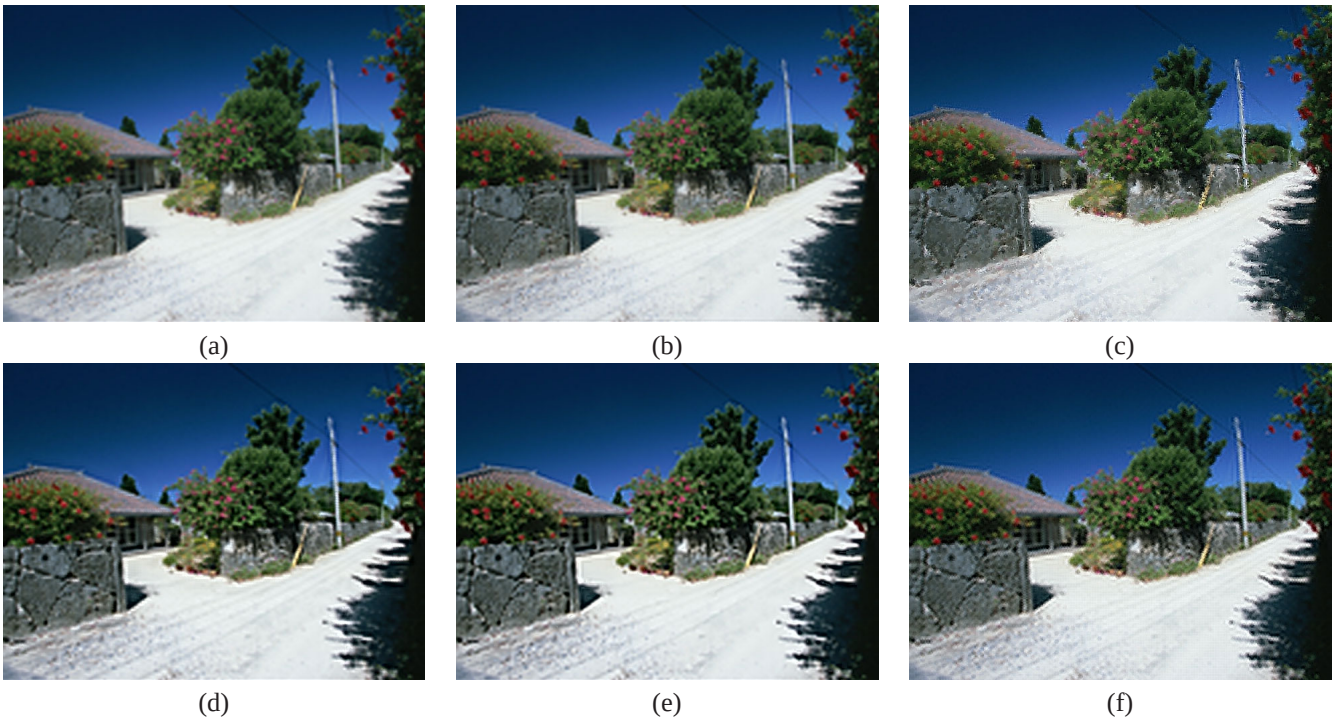

Fig. 6. Comparison of results (640×480 pixels) obtained by using different image enlargement methods (Test image 3): (a) Result of reconstruction by sinc interpolation, (b) Result of reconstruction by the local-PCA based method, (c) Result of reconstruction by the conventional method [16], (d) Result of reconstruction by the conventional method [12], (e) Result of reconstruction by the conventional method [29], (f) Result of reconstruction by the proposed method.

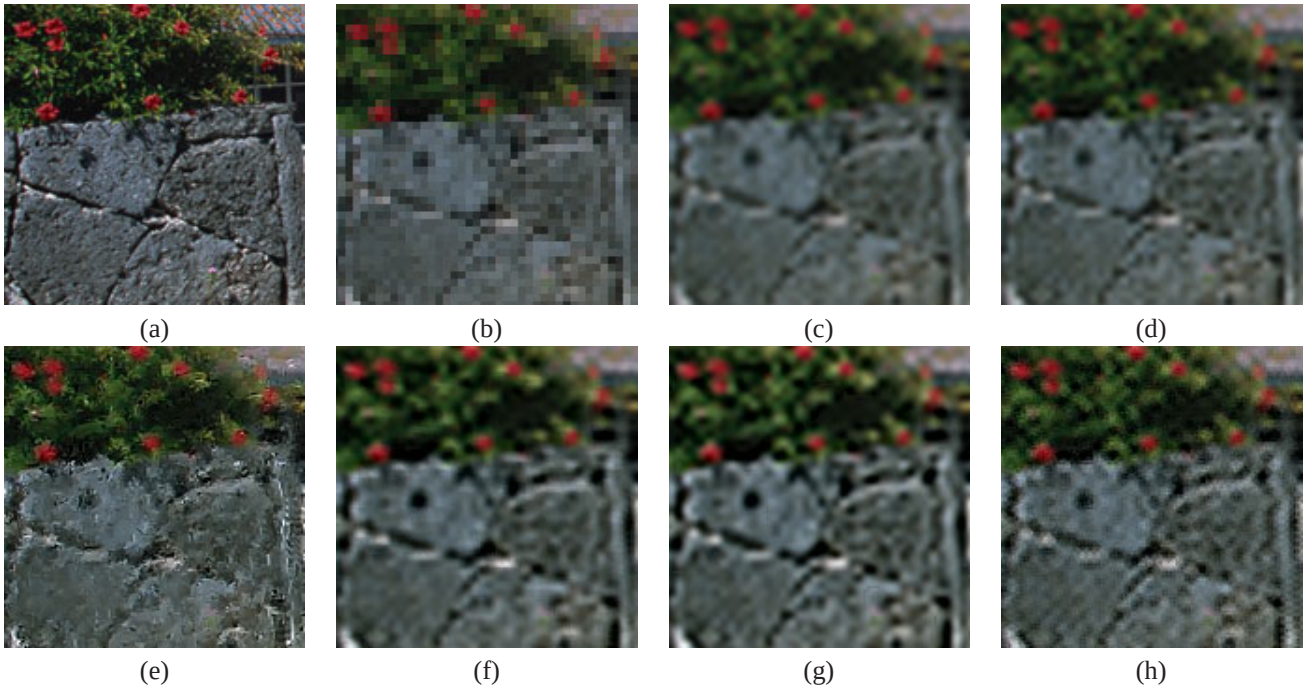

Fig. 7. (a) Zoomed portion of Fig. 2(c), (b) Zoomed portion of Fig. 2(g), (c) Zoomed portion of Fig. 6(a), (d) Zoomed portion of Fig. 6(b), (e) Zoomed portion of Fig. 6(c), (f) Zoomed portion of Fig. 6(d), (g) Zoomed portion of Fig. 6(e), (h) Zoomed portion of Fig. 6(f).

is a test texture image (480×359 pixels, 24-bit color levels) that includes the text "Grand Canyon", and it is obtained from Fig. 9(a). For comparison, we utilized the method in [10], the local-PCA based method, the kernel PCA-based method using [12], and the sparse representation based method [32]. The conventional method [10] performs the restoration of missing areas by using PCA, and the local-PCA based method utilizes PCA with the texture classification scheme, i.e., this method is a simple PCA-based version of the proposed method without using the kernel method. Furthermore, the

Fig. 8. Comparison of results by the conventional and proposed methods (Test image 4): (a) Zoomed portion of Fig. 2(d), (b) Zoomed portion of Fig. 2(h), (c) Zoomed portion of reconstruction result by sinc interpolation, (d) Zoomed portion of reconstruction result by the local-PCA based method, (e) Zoomed portion of reconstruction result by the conventional method [16], (f) Zoomed portion of reconstruction result by the conventional method [12], (g) Zoomed portion of reconstruction result by the conventional method [29], (h) Zoomed portion of reconstruction result by the proposed method.

conventional method based on [12] uses the projection to the nonlinear eigenspace obtained by kernel PCA for the restoration. Thus, we utilized these three methods for the comparison of the proposed method. In addition, the conventional method in [32] is a representative one which realizes the missing area restoration using the sparse representation, and it is the existing state of the art. Thus, we also added this method to the experiments. Figures 10(b)–(e) show the results of

(a) (b) (c)

Fig. 9. Three texture images utilized in the verification of missing area restoration performance: (a) Original test image 1 of size 480×359 pixels, (b) Original test image 2 of size 480×360 pixels, (c) Original test image 3 of size 480×360 pixels.

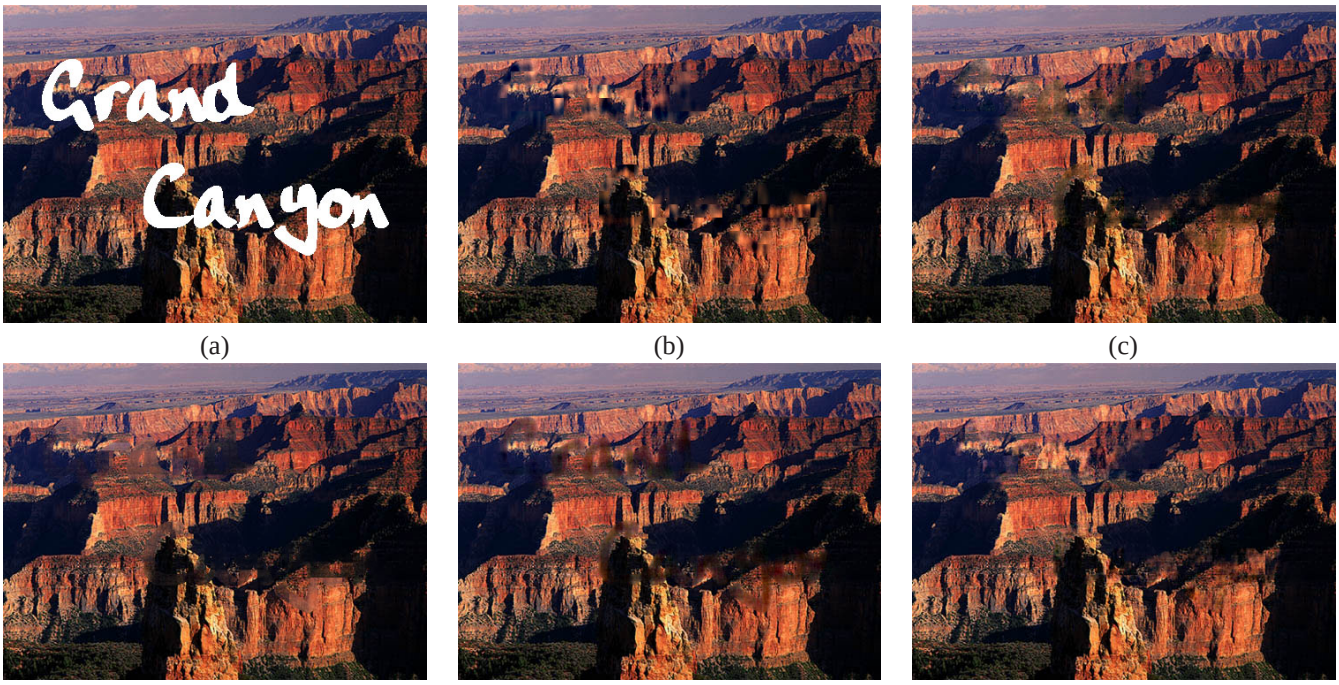

(a) (b) (c)

(d) (e) (f)

Fig. 10. Comparison of results obtained by using different missing area restoration methods (Test image 1): (a) Corrupted image including text regions "Grand Canyon" (8.9 % loss), (b) Image reconstructed by the conventional method [10], (c) Image reconstructed by the local-PCA based method, (d) Image reconstructed by the kernel PCA based method using [12], (e) Image reconstructed by the conventional method [32], (f) Image reconstructed by the proposed method.

TABLE II
IMAGE ENLARGEMENT PERFORMANCE COMPARISON (SSIM) OF THE PROPOSED METHOD AND THE CONVENTIONAL METHODS.

Test image	Sinc interpolation	Local PCA	Reference [16]	Reference[12]	Reference [29]	**Proposed method**
Fig. 2(a)	0.8172	0.8345	0.7735	0.8376	0.8276	**0.8467**
Fig. 2(b)	0.7970	0.8091	0.7334	0.8008	0.7789	**0.8153**
Fig. 2(c)	0.6983	0.7175	0.6176	0.7190	0.7146	**0.7440**
Fig. 2(d)	0.5062	0.5502	0.3973	0.5733	0.5580	**0.6260**

reconstruction by the above four conventional methods, and Fig. 10(f) shows the result by the proposed method. In this simulation, we set the parameters of the proposed method as follows: the size of local images ($w \times h$ pixels) was set to a tenth of the target image size, and $\tilde{w}_1 = \frac{w}{6}$, $\tilde{h}_1 = \frac{h}{6}$, $\tilde{w}_2 = \frac{w}{4}$, $\tilde{h}_2 = \frac{h}{4}$, $K = 6$, and Th = 0.8. Note that for color images, the proposed method and the conventional methods calculate vectors that contain RGB component values within local images and perform their reconstruction.

As shown in the previous subsection, the proposed method introduces the kernel PCA and the new classification scheme into the POCS algorithm. Then these two schemes provide the solutions to the problems of the conventional methods causing the over-smoothness and the degradation due to different kinds

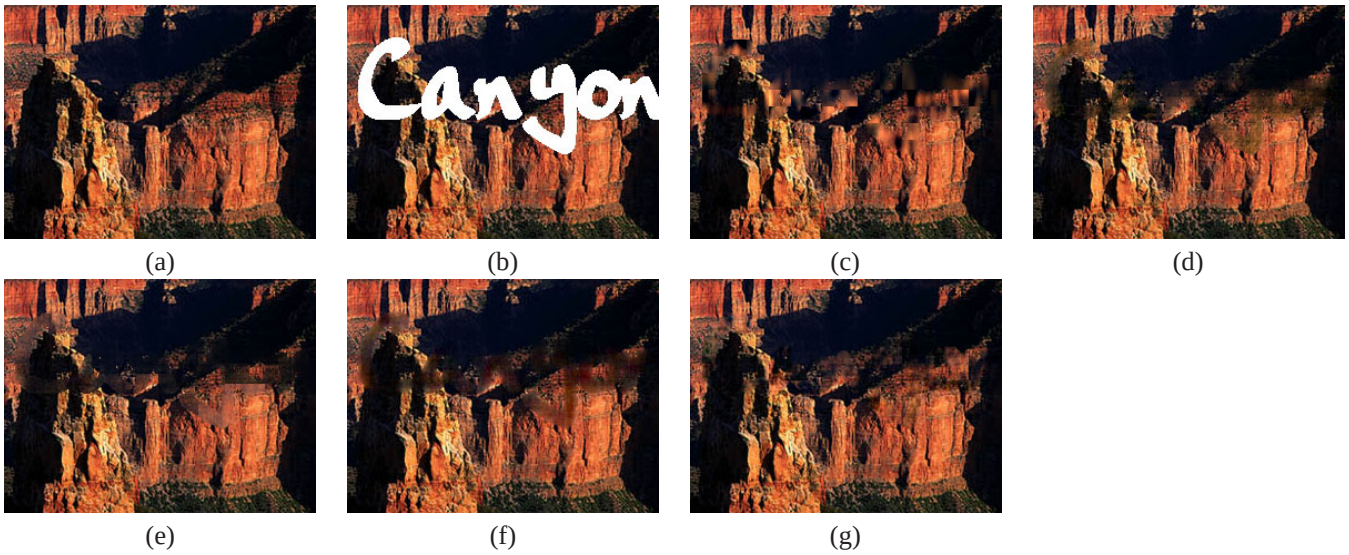

Fig. 11. (a) Zoomed portion of Fig. 9(a), (b) Zoomed portion of Fig. 10(a), (c) Zoomed portion of Fig. 10(b), (d) Zoomed portion of Fig. 10(c), (e) Zoomed portion of Fig. 10(d), (f) Zoomed portion of Fig. 10(e), (g) Zoomed portion of Fig. 10(f).

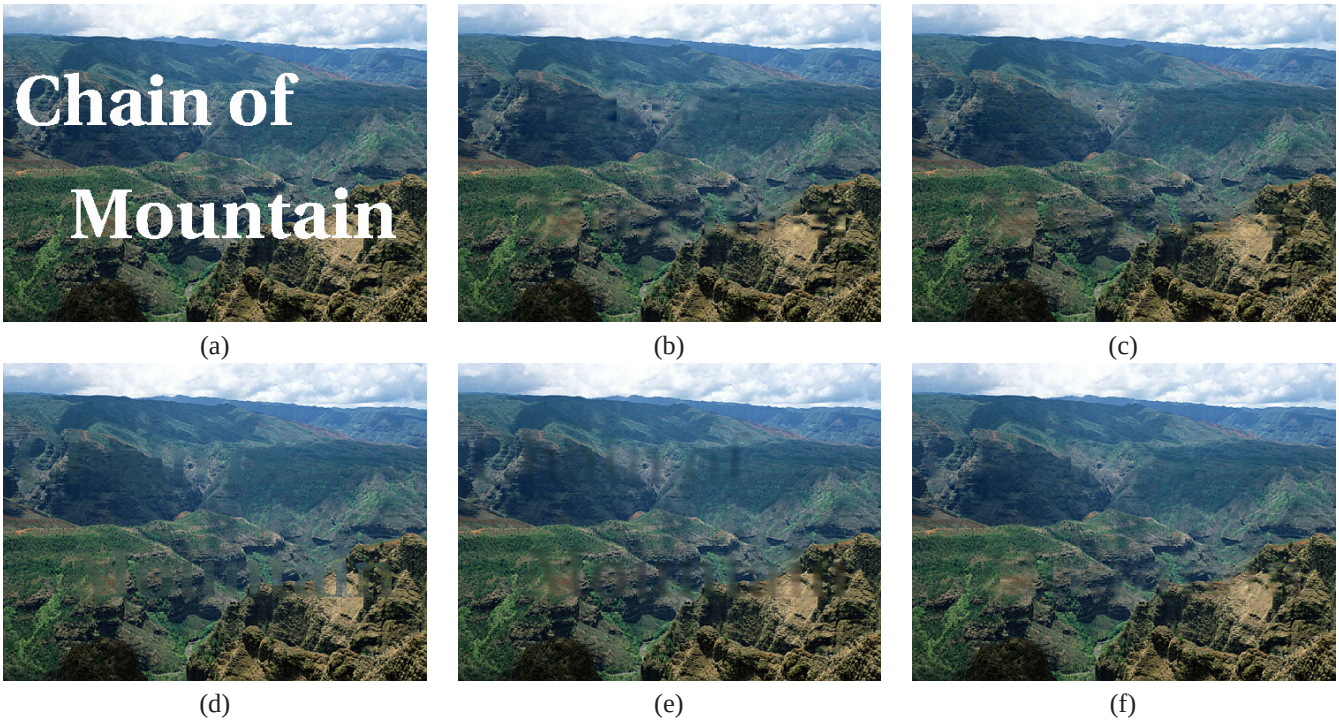

Fig. 12. Comparison of results obtained by using different missing area restoration methods (Test image 2): (a) Corrupted image including text regions "Chain of Mountain" (8.9 % loss), (b) Image reconstructed by the conventional method [10], (c) Image reconstructed by the local-PCA based method, (d) Image reconstructed by the kernel PCA based method using [12], (e) Image reconstructed by the conventional method [32], (f) Image reconstructed by the proposed method.

of textures. Therefore, as shown in Figs. 10 and 11, the proposed method provides higher performance than those of the conventional methods.

Different experimental results are shown in Figs. 12–15. Compared to the results obtained by using the conventional methods, it can be seen that various kinds of textures can be restored by the proposed method, successfully. Furthermore, in order to quantitatively compare the proposed method and the conventional methods, we show the PSNR and the SSIM index of the obtained results in Tables III and IV. Note that in the proposed method and the conventional methods, missing areas are restored for each local image. Therefore, we show the average values of the PSNR and the SSIM index obtained from those local images. From Table IV, the proposed method achieves noticeable improvement over the conventional methods in the SSIM index. In Table III, the PSNR has similar problems shown in the previous subsection, and it cannot reflect the perceptual quality. Then from the

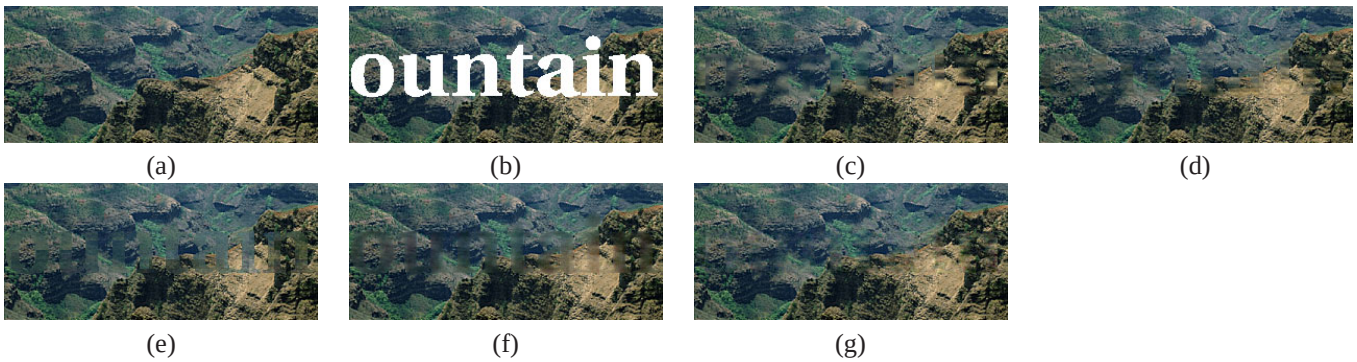

Fig. 13. (a) Zoomed portion of Fig. 9(b), (b) Zoomed portion of Fig. 12(a), (c) Zoomed portion of Fig. 12(b), (d) Zoomed portion of Fig. 12(c), (e) Zoomed portion of Fig. 12(d), (f) Zoomed portion of Fig. 12(e), (g) Zoomed portion of Fig. 12(f).

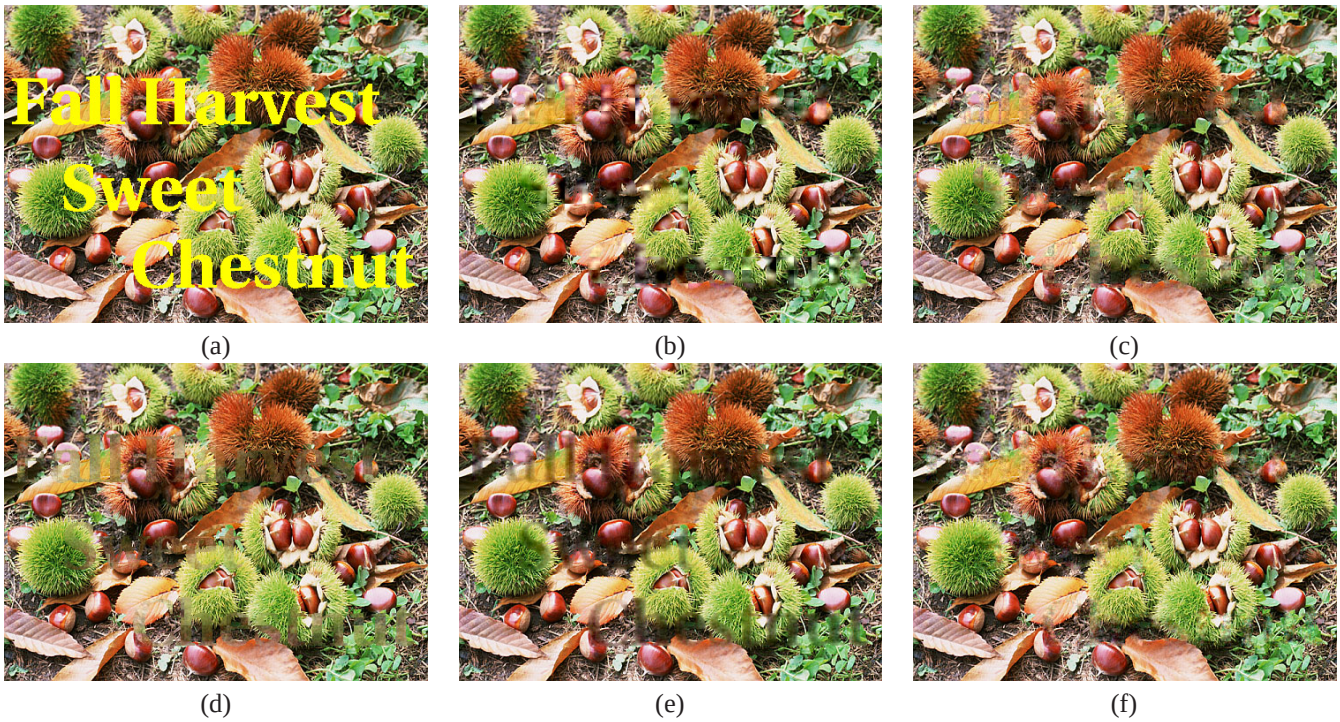

Fig. 14. Comparison of results obtained by using different missing area restoration methods (Test image 3): (a) Corrupted image including text regions "Fall Harvest Sweet Chestnut" (11.3 % loss), (b) Image reconstructed by the conventional method [10], (c) Image reconstructed by the local-PCA based method, (d) Image reconstructed by the kernel PCA based method using [12], (e) Image reconstructed by the conventional method [32], (f) Image reconstructed by the proposed method.

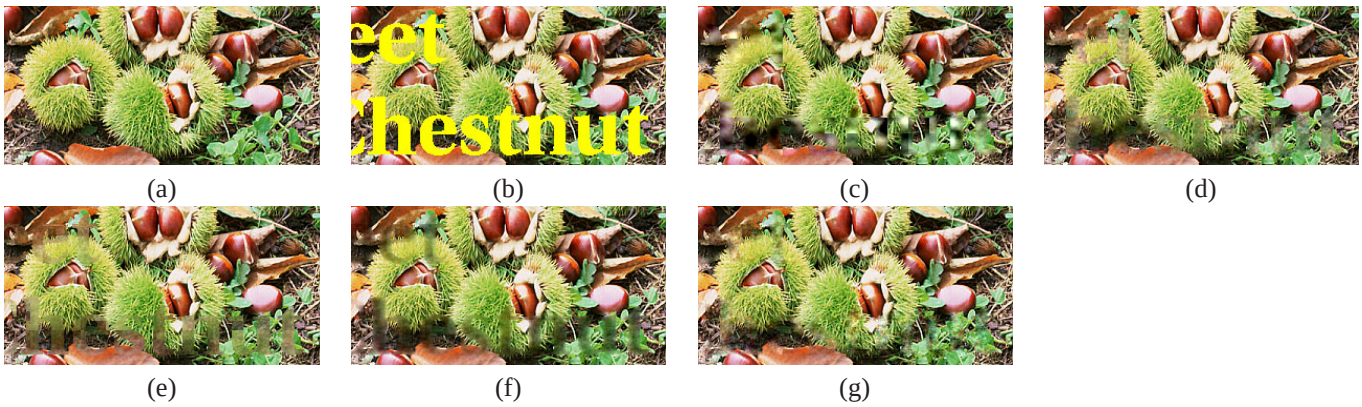

Fig. 15. (a) Zoomed portion of Fig. 9(c), (b) Zoomed portion of Fig. 14(a), (c) Zoomed portion of Fig. 14(b), (d) Zoomed portion of Fig. 14(c), (e) Zoomed portion of Fig. 14(d), (f) Zoomed portion of Fig. 14(e), (g) Zoomed portion of Fig. 14(f).

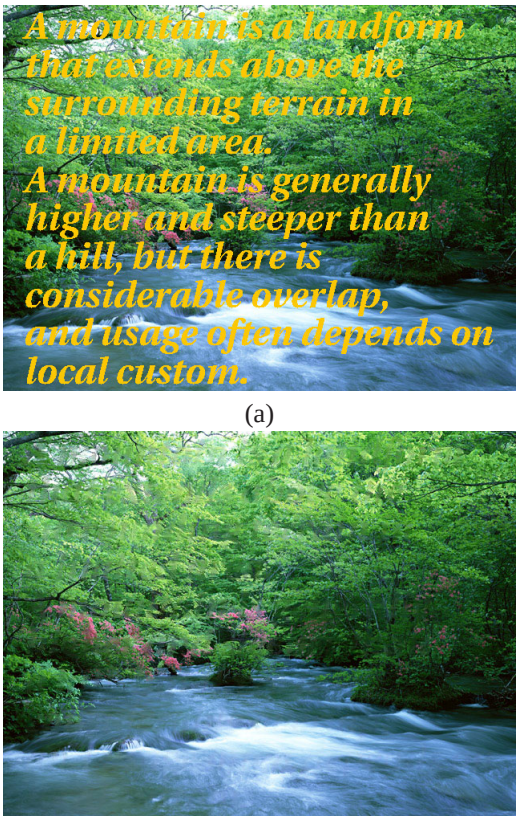

(a)

(b)

Fig. 16. Example of restoration by the proposed method for image including text regions in the whole areas: (a) Corrupted image (640×480 pixels, 18.5 % loss), (b) Image reconstructed by the proposed method.

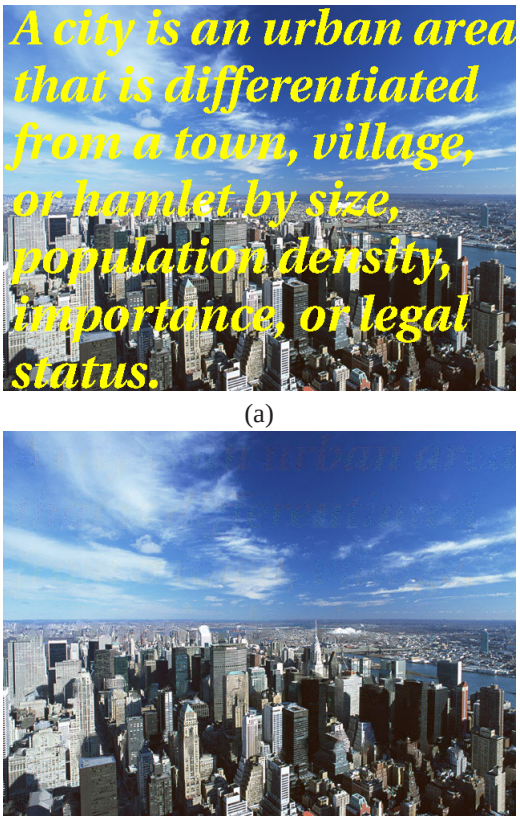

(a)

(b)

Fig. 17. Other example of restoration by the proposed method for image including text regions in the whole areas: (a) Corrupted image (640×480 pixels, 17.6 % loss), (b) Image reconstructed by the proposed method.

evaluation based on the SSIM index, we can see our method also realizes successful missing area restoration subjectively and quantitatively.

Finally, in Figs. 16 and 17, we show some examples of restoration by the proposed method for images including text regions in the whole areas. From these figures, we can see the proposed method restores several kinds of missing ares, and many applications such as removal of unnecessary objects and error concealment can be expected.

VI. CONCLUSIONS

In this paper, we have presented a new missing intensity interpolation method using a kernel PCA-based POCS algorithm and its applications. In order to realize accurate reconstruction of images containing several kinds of texture, the proposed method first introduces a nonlinear eigenspace calculated for each kind of texture within the target image into the constraint of the POCS algorithm. Furthermore, an adaptive selection scheme of the optimal eigenspace based on the converged errors of the POCS algorithm enables each missing texture in the target image to be reconstructed successfully. Finally, since our algorithm can interpolate arbitrary-shaped missing areas, the potential of our algorithm in two image reconstruction tasks, image enlargement and missing area restoration, is also demonstrated in this paper.

In this study, we manually set parameters such as the size of local images and number of clusters. It is desirable that these values can be adaptively determined from the observed images. Thus, we need to complement this determination algorithm. We would like to study these ideas for interpolation in video data. These topics will be the subject of subsequent reports.

ACKNOWLEDGMENT

This work was partly supported by Grant-in-Aid for Scientific Research (B) 21300030, Japan Society for the Promotion of Science (JSPS).

REFERENCES

[1] H.S. Hou, H.C. Andrews, "Cubic splines for image interpolation and digital filtering," *IEEE Trans. on Acoustics, Speech, Signal Processing* ASSP-26 (6) pp.508–517, 1978.

[2] R.G. Keys, Cubic convolution interpolation for digital image processing, *IEEE Trans. on Acoustics, Speech, Signal Processing*, 29 (6) pp.1153–1160, 1981.

[3] F. Arandiga,R. Donat, P. Mulet, "Adaptive interpolation of images," *Signal Processing*, vol.83, no.2, pp.459-64, 2003.

[4] S. Battiato, G. Gallo, F. Stanco, "A locally adaptive zooming algorithm for digital images," *Image and vision computing*, vol.20, no.11, pp.805–812, 2002.

[5] C. Ballester, M. Bertalmio, V. Caselles, G. Sapiro, "Filling-In by Joint Interpolation of Vector Fields and Gray Levels," *IEEE Trans. on Image Processing*, vol.10, no.8, pp.1200–1211, 2001.

[6] T.F. Chan and Jianhong Shen, "Nontexture inpainting by curvature-driven diffusions," *Journal of Visual Communication and Image Representation*, vol.12, no.4, pp.436–449, 2001.

TABLE III
MISSING AREA RESTORATION PERFORMANCE COMPARISON (PSNR) OF THE PROPOSED METHOD AND THE CONVENTIONAL METHODS.

Test image	Reference [10]	Local PCA	Kernel PCA based method using [12]	Reference [32]	**Proposed method**
Fig. 9(a)	25.70	27.68	26.53	26.73	**26.37**
Fig. 9(b)	29.56	30.51	29.98	30.39	**30.13**
Fig. 9(c)	21.86	23.05	22.20	22.43	**22.67**

TABLE IV
MISSING AREA RESTORATION PERFORMANCE COMPARISON (SSIM) OF THE PROPOSED METHOD AND THE CONVENTIONAL METHODS.

Test image	Reference [10]	Local PCA	Kernel PCA based method using [12]	Reference [32]	**Proposed method**
Fig. 9(a)	0.9257	0.9321	0.9262	0.9324	**0.9384**
Fig. 9(b)	0.9318	0.9314	0.9309	0.9384	**0.9475**
Fig. 9(c)	0.9042	0.9035	0.8959	0.9063	**0.9323**

[7] A. Rares, M.J.T. Reinders, and J. Biemond, "Edge-based image restoration," *IEEE Trans. on Image Processing*, vol.14, no.10, pp.1454–1468, 2005.

[8] A. A. Efros and T. K. Leung, "Texture synthesis by nonparametric sampling," *IEEE Int. Conf. Computer Vision*, Corfu, Greece, pp.1033–1038, Sept. 1999.

[9] A. Kokaram, "A statistical framework for picture reconstruction using 2D AR models," *Image and Vision Computing*, vol.22, no.2, 1, pp.165–171, Feb. 2004.

[10] T. Amano and Y. Sato, "Image interpolation using BPLP method on the eigenspace," *Systems and Computers in Japan*, vol.38, no.1, pp.87–96, Jan. 2007.

[11] B. Schölkopf, S. Mika, C.J.C Burges, P. Knirsch, K.-R. Müller, G. Rätsch, and A.J. Smola, "Input space versus feature space in kernel-based methods," *IEEE Trans. on Neural Networks*, vol.10, no.5, pp.1000–1017, 1999.

[12] K.I. Kim, M.O. Franz , B. Schölkoph, "Iterative kernel principal component analysis for image modeling," *IEEE Trans. on Pattern Analysis and Machine Intelligence*, vol.27, no.9, pp.1351–1366, 2005.

[13] C.V. Jiji, S. Chaudhuri, and P. Chatterjee "Single frame image super-resolution: should we process locally or globally?," *Multidimensional Systems and Signal Processing*, vol.18, no.2–3, Sept., pp.123–125, 2007.

[14] A. Hertzmann, C.E. Jacobs, N. Oliver, B. Curless, and D.H. Salesin, "Image Analogies," *Computer Graphics (Proc. Siggraph 2001)*, pp. 327–340, 2001.

[15] W. T. Freeman, E. C. Pasztor, and O. T. Carmichael, "Learning low-level vision", *International Journal of Computer Vision*, vol. 40, no. 1, pp. 25–47, 2000.

[16] W.T. Freeman, T.R. Jones, and E.C. Pasztor, "Example-based super-resolution," *IEEE Computer Graphics and Applications*, 22(2), pp. 56–65, 2002.

[17] T. A. Stephenson and T. Chen, "Adaptive Markov Random Fields for example-based super-resolution of faces," *EURASIP Journal on Applied Signal Processing*, vol.2006, no.1, pp.225–225, 2006.

[18] Q. Wang, X. Tang, and H. Shum, "Patch based blind image super resolution," *ICCV 2005*, vol.1, pp.709–716, 2005.

[19] X. Li, K.M. Lam, G. Qiu, L. Shen, and S. Wang, "An Efficient Example-Based Approach for Image Super-Resolution," *ICNNSP 2008*, pp.575–580, 2008.

[20] J. Sun, N. Zheng, H. Tao, and H. Shum, "Image hallucination with primal sketch priors," *IEEE CVPR 2003*, vol.2, pp.729–736, 2003.

[21] C.V. Jiji, M.V. Joshi, S. Chaudhuri, "Single-frame image super-resolution using learned wavelet coefficients," *International Journal of Imaging Systems and Technology*, vol.14, no.3, pp.105–112, 2004.

[22] C.V. Jiji and S. Chaudhuri, "Single-frame image super-resolution through contourlet learning," *EURASIP Journal on Applied Signal Processing*, vol.2006, no.10, pp. 1–11, 2006.

[23] X. Wang and X. Trang, "Hallucinating face by eigentransformation," *IEEE Transactions on Systems, Man, and Cybernetics*, vol.35, no.3, pp.425–434, 2005.

[24] A. Chakrabarti, A.N. Rajagopalan, and R. Chellappa, "Super-resolution of face images using kernel PCA-based prior," *IEEE Transactions on Multimedia*, vol.9, no.4, pp.888–892, 2007.

[25] S. Chaudhuri and M.V. Joshi, "Motion-free super-resolution," *New york: Springer*, 2005.

[26] M. Turk and A. Pentland, "Eigenfaces for recognition," *Journal of Cognitive Neuroscience*, 3(1), pp.71–86, 1991.

[27] C. Bishop, A. Blake, and B. Marthi, "Super-resolution enhancement of video," *Artificial Intelligence and Statistics (AISTATS)*, 2003.

[28] K.I. Kim, Y. Kwon, "Example-Based Learning for Single-Image Super-Resolution," *Lecture Notes in Computer Science, Pattern Recognition - 30th DAGM Symposium, Proceedings*, pp.456–465, 2008.

[29] Y. Hu, T. Shen, K.M. Lam, and S. Zhao, "A Novel Example-Based Super-Resolution Approach Based on Patch Classification and the KPCA Prior Model," *Computational Intelligence and Security 2008*, vol. 1, pp.6–11, 2008.

[30] M. Aharon, M. Elad, A. Bruckstein, "K-SVD: An algorithm for designing overcomplete dictionaries for sparse representation," *IEEE Trans. Signal Process.*, vol.54, no.11, 2006.

[31] M. Elad and M. Aharon, "Image denoising via sparse and redundant representations over learned dictionaries," *IEEE Trans. on Image Processing*, vol. 15, no. 12, 2006.

[32] J. Mairal, M. Elad, and G. Sapiro, "Sparse representation for color image restoration," *IEEE Trans. on Image Processing*, vol.17, no.1, 2008.

[33] D. C. Youla and H. Webb, "Image restoration by the method of convex projections: Part 1 – Theory," *IEEE Trans. Medical Imaging*, vol.MI-1, pp.81–94, Oct. 1982.

[34] T. Ogawa, M. Haseyama, "POCS-based texture reconstruction method using clustering scheme by kernel PCA," *IEICE Trans. Fundamentals*, vol. E90-A, no. 8, pp. 1519–1527, Aug. 2007.

[35] J.T.Y. Kwok, and I.W.H. Tsang, "The pre-image problem in kernel methods," *IEEE Trans. on Neural Networks*, vol.15, no.6, pp.1517–1525, 2004.

[36] Z. Wang, A.C. Bovik, H.R. Sheikh, and E.P. Simoncelli, "Image quality assessment: From error visibility to structural similarity," *IEEE Transactions on Image Processing*, vol. 13, no. 4, pp. 600–612, Apr. 2004.

Takahiro Ogawa received his B.S., M.S. and Ph.D. degrees in Electronics and Information Engineering from Hokkaido University, Japan in 2003, 2005 and 2007, respectively. He is currently an assistant professor in the Graduate School of Information Science and Technology, Hokkaido University. His research interests are digital image processing and its applications. He is a member of the IEEE, EURASIP,IEICE, and Institute of Image Information and Television Engineers (ITE).

Miki Haseyama received her B.S., M.S. and Ph.D. degrees in Electronics from Hokkaido University, Japan in 1986, 1988 and 1993, respectively. She joined the Graduate School of Information Science and Technology, Hokkaido University as an associate professor in 1994. She was a visiting associate professor of Washington University, USA from 2005 to 2006. She is currently a professor in the Graduate School of Information Science and Technology, Hokkaido University. Her research interests include image and video processing and its development into semantic analysis. She is a member of the IEEE, IEICE, Institute of Image Information and Television Engineers (ITE) and Acoustical Society of Japan (ASJ).